Available at www.sciencedirect.com

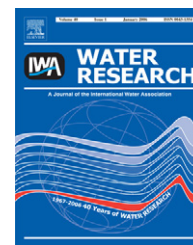**ScienceDirect**

journal homepage: www.elsevier.com/locate/watres

Oxygen diffusion in active layer of aerobic granule with step change in surrounding oxygen levels

Z.C. Chiu[a], M.Y. Chen[a], D.J. Lee[a,*], C.H. Wang[b], J.Y. Lai[c]

[a]Department of Chemical Engineering, National Taiwan University, No. 43, Sector 4, Keelung Road, Taipei 10617, Taiwan
[b]Department of Chemical and Biomolecular Engineering, National University of Singapore; 4 Engineering Drive 4, Singapore 117576, Singapore
[c]Department of Chemical Engineering, R&D Center of Membrane Technology, Chung Yuan Christian University, Chungli 32023, Taiwan

A B S T R A C T

High biomass density and large size limit the transfer of dissolved oxygen (DO) in aerobic granules. In the literature, the oxygen diffusivity is often employed as an input parameter for modeling transport processes in aerobic granules. The interior of an aerobic granule was observed to be highly heterogeneous. In this work, the distributions of extracellular polymeric substances (EPS) and cells in the interior of phenol-fed and acetate-fed granules were built up using a five-fold staining scheme, combined with the use of a confocal laser scanning microscope (CLSM). The steady-state and transient DO with step changes in surrounding DO levels at various depths were measured in the granules using microelectrodes. Cells were probed in a surface layer of thickness 125–375 μm. A marked fall in DO was also noted over this surface layer. No aerobic oxidation could occur beneath the active layer, indicating the oxygen transfer limit. Fitting the steady-state and transient DO data over the active surface layer yielded apparent diffusivities of oxygen were $(9.5 \pm 3.5) \times 10^{-10}\, m^2\, s^{-1}$ for the phenol-fed granule and $(3.5 \pm 1.0) \times 10^{-10}\, m^2\, s^{-1}$ for the phenol-fed granule. These values were lower than those adopted in models in the literature.

1. Introduction

Granulation in aerobic systems has been widely studied (Beun et al., 2002; Mulder et al., 2001; Tay et al., 2002a, b). The aerobic granule system has a very high biomass concentration (up to $15\, g\, l^{-1}$) (Di Iaconi et al., 2005) and can degrade high-strength wastewater (to $15\, kg\, COD/m^3\, d$) (Moy et al., 2002).

During pollutant oxidation, the organic pollutant and dissolved oxygen (DO) are initially transferred from the bulk liquid to the external surface of the granule, before diffusing or being carried by an advective flow into the interior for oxidation. Morgenroth et al. (1997) assumed that the center of the granules is anaerobic, although the surrounding liquid

has a relatively high DO content. Liu et al. (2005) noted a decline in specific substrate removal rate from large granules, revealing the inhibition induced by mass transfer resistance. Oxygen limitation, if occurred, produced anaerobic core in aerobic granule. Anaerobic bacteria were noted to exist in the anaerobic core for large aerobic granules (Ivanov et al., 2004).

Oxygen diffusivity is commonly applied as an input parameter for modeling the transport processes in bioaggregates. For example, Li and Bishop (2004) assumed that the oxygen diffusivity in their biofilm model was 20% lower than that in pure water at $1.79 \times 10^{-9}\, m^2\, s^{-1}$ at 20 °C. Li and Liu (2005) assumed $D_{app} = 2.0 \times 10^{-9}\, m^2\, s^{-1}$ for oxygen in their granule model, and then concluded that in granules with radii

*Corresponding author. Tel.: +886 2 23625632; fax: +886 2 23623040.
E-mail address: djlee@ntu.edu.tw (D.J. Lee).

of over 0.5 mm, the oxygen limitation effects can be significant. The critical diameter of granule, above which anaerobic core would be present in granule is an important parameter for determining the optimal size of granule. Using a confocal laser scanning microscope (CLSM), Tay et al. (2003) found that critical diameter could be around 1.6–1.7 mm. Considering the position where live cells were present in a granule, the critical diameter would be around 1 mm (Toh et al., 2002).

Recently, the microelectrode method has been adopted to evaluate the micro-transport processes in aerobic granules (Jang et al., 2003). Cronenberg and Van Den Heuvel (1991) proposed the use of a microelectrode to probe the change in concentration of glucose at the center of a biofilm that was subjected to a stepwise change in bulk concentration, and thus extract the diffusion coefficient of glucose in a biofilm from the time sequence data when the biofilm was inactive. Beuling et al. (2000) proposed that, at another extreme when the entire biofilm was active and exhibited the same reaction rates over the film, the diffusion coefficient data could also be acquired by tracking the local response of species under a sudden change in bulk concentrations. Chiu et al. (2006) were the first to estimate the oxygen diffusivity in acetate-fed and phenol-fed aerobic granules by probing the DO level at the granule center using microelectrodes with a sudden change in the DO of the bulk liquid. The flow velocity across the granule was set such that the external mass transfer resistance was negligible. The granules were stored at 4 °C and were tested immediately after the temperature recovered to room temperature, to allow a much lower chemical reaction rate than the diffusion rate of oxygen. Then, the oxygen diffusivity of the aerobic granule was estimated with reference to a one-dimensional diffusion model that considers only internal mass transfer resistance. The diffusivity thus found ranges from 1.24 to $2.28 \times 10^{-9}\,m^2\,s^{-1}$ for acetate-fed granules of size 1.28–2.50 mm, and 2.50–$7.65 \times 10^{-10}\,m^2\,s^{-1}$ for phenol-fed granules of size 0.42–0.78 mm. Chu et al. (2005) adopted the same fitting technique to estimate oxygen diffusivity in wastewater sludge flocs.

Tay et al. (2002c) noted that the interior of aerobic granules was not uniform, but in layered. McSwain et al. (2005) proposed that protein content is high in the core of the granule, and its presence facilitates granulation and promotes stability. Wang et al. (2005) noted a granule core full of loosely structured substances, surrounded by β-linked polysaccharides in a dense, outer layer with a thickness of 200–300 μm, which ensured the structural stability of the granules. Hence, the granule interior should not be modeled as a uniform porous medium, as was assumed by Chiu et al. (2006). The oxygen diffusivity of active layers in aerobic granule based on its real architecture is needed for comprehensive modeling. This work probes the distributions of extracellular polymeric substances (EPS) and cells within the granule interior by a five-fold staining scheme, and recorded the transient and steady-state DO levels at various depths in the *same* granule by microelectrodes with stepwise change in surrounding DO level. The diffusivity of oxygen of the layers of high bioactivity in granules was then estimated using a simplified one-dimensional diffusion-reaction model.

2. Experimenal

2.1. Samples

The phenol-fed granules were cultivated for three months in a column-type (120 cm height; 5 cm diameter) reactor with a working volume of 2 l. The reactor was aerated with an airflow rate of superficial velocity of 2.5 mm s^{-1}. Synthetic wastewater containing phenolic compound similar to Jiang et al. (2002) was applied to cultivate the granules at a phenol concentration of 500 mg l^{-1}. The reactors operated sequentially in 4-h cycles. The phase duration of a typical 4-h working cycle included 2 min of influent filling, 213–229 min of aeration, 4–20 min of settling and 5 min of effluent withdrawal at a volumetric exchange ratio of 50%. The microphotograph of the tested phenol granule is shown in Fig. 1a.

The acetate-fed granules were incubated for 3 months in a column-type sequential aerobic sludge blanket reactor with a working volume of 2.5 l. The reactor was fed with the seed sludge and an acetate-based synthetic wastewater with mineral compositions half concentrations to Tay et al. (2001). This synthetic wastewater had acetate as the sole carbon source and an acetate concentration of 1000 mg l^{-1}. Air bubbles were supplied at superficial velocity of 2 cm s^{-1}. The reactor was operated sequentially with 4 min of influent
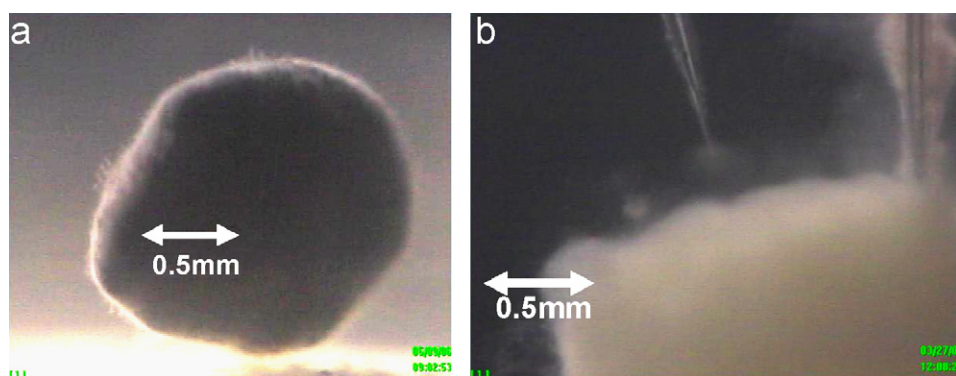

Fig. 1 – Microphotographs of the tested granules: (a) phenol-fed granule; diameter = 1.7 mm and (b) acetate-fed granule; diameter = 3.1 mm.

filling, 202 min of aeration, 30 min of settling and 4 min of effluent withdrawal.

2.2. Measurements using microelectrodes

A 10 μm diameter DO microelectrode (DO-1, Unisense, Denmark) was employed to track the time evolution of the local DO concentration at different depths in the granule. A micromanipulator was used to adjust finely the position of the electrode tip at a spatial resolution of better than 20 μm. The stirring sensitivity of the sensor was less than 2%, and its response time (90%) was less than 3 s. The output of the sensor was recorded using a picoammeter (PA2000, Unisense, Denmark) and a personal computer. The signals from the microsensors were transformed to DO concentrations in μmol l^{-1}. Calibration to microelectrode measurement was made before and after each granule test.

The flow chamber used by Chiu et al. (2006), modified from that of Li and Bishop (2004), was applied to maintain the granule physically in a stream of flowing water (Fig. 1 in Chiu et al. (2006)). The granule was extracted carefully using a wide-mouth pipette and one DO microelectrode (#2) was placed at the center of the granule and another, identical DO microelectrode, outside the granule (#1). The incoming water stream was switched between the distilled water saturated with oxygen (stream #A) and the distilled water whose oxygen content was reduced by continuous nitrogen-gas purging (stream #B). Restated, although the two kinds of granules tested were cultivated at different aeration rates, the testing procedures with step changes in surrounding DO levels were identical. The DO signals were collected at 10 s intervals to yield transient and steady-state data. Then, electrode #1 was moved from the bulk towards the granule. This procedure was repeated and the DO signals from the microelectrodes #1 and #2 were recorded at different depths with stepwise changes in surrounding DO level.

2.3. Staining and CLSM imaging

The granules after microelectrode tests were collected and kept fully hydrated for staining. We applied a five-fold staining scheme for probing the proteins, cells (total and dead), and α- and β-polysaccharides. The calcofluor white was purchased from Sigma (St. Louis, USA). FITC, Con A conjugated with tetramethylrhodamine, SYTO 63, and SYTOX blue were from Molecular Probes (Carlsbad, CA, USA).

In staining, SYTO 63 (20 μM) was initially dripped onto the sample, which was placed on a shaker table for 30 min. Next, 0.1 M sodium bicarbonate buffer was added to the sample to maintain the amine group in non-protonated form. Then, the FITC solution (10 g l^{-1}) was added to the sample for 1 h at room temperature. Then, the Con A solution (250 mg l^{-1}) was added to the sample and incubated for another 30 min. Calcofluor white (fluorescent brightener 28, 300 mg l^{-1}) was then used to stain the β-linked D-glucopyranose polysaccharides for 30 min. After each of the aforementioned four staining stages, the stained sample was washed twice to remove extra stain by phosphate buffered saline (PBS). The stained sample was stored at 4 °C. Before observation, the SYTOX Blue solution was added to the samples for incubation for 5 min.

The stained granules were embedded for cryosectioning and frozen at −20 °C. Then, 60 μm sections were cut on a cryomicrotome and mounted onto microscopic slides for observation (Chu et al., 2004; Chu et al., 2005).

2.4. CLSM imaging

To probe the internal structure of granules, the confocal laser scanning microscopy (CLSM; Leica TCS SP2 Confocal Spectral Microscope Imaging System, Germany) was used. The granule was imaged with a 10× or 20× objective and analyzed with the Leika confocal software. The fluorescence of SYTO 63 was detected by excitation at 633 nm and emission at 650–760 nm (red). Excitation at 543 nm and emission at 550–590 nm (light blue) was used to detect Con A conjugates. The FITC probe was detected by excitation at 488 nm and emission 500–540 nm (green). The fluorescent intensity of SYTOX Blue was detected by excitation at 458 nm and emission at 460–500 nm (purple). The fluorescence of calcofluor white was detected by excitation at 405 nm and emission width at 410–480 nm (blue). Both SYTO 63 and FITC were detected together and others were detected individually.

3. Results

3.1. DO levels and CLSM images for phenol-fed granule

Fig. 2 plots the DO concentrations measured at various positions outside and inside a phenol-fed granule (Fig. 1a) using microelectrodes #1 and #2. The diameter of the granule was 1.70 mm and the upflow velocity was 2.5 mm s^{-1}, giving a Reynolds number of 4.2. The DO detected at 0.5 mm from granule surface switched between those in bulk stream #A (250–270 μmol l^{-1}) and in bulk stream #B (120–150 μmol l^{-1}). The DO concentrations of surrounding liquid decreased with distance to the granules, indicating the presence of external mass transfer resistance of oxygen through the boundary layer. On the granule surface, the DO declined to approximately 80% of that of the bulk liquid. The DO decreased monotonically with distance into the granule. When the bulk water was saturated with oxygen (stream #A), the DO ranged 40–60 μmol l^{-1} at a depth of 125 μm, and further declined to zero at a depth of 200 μm and greater. When the DO level in the bulk water was fell (stream #B, 120–150 μmol l^{-1}), the local DO inside granule was zero at a depth of 125 μm. Whether the granule has an anaerobic core, as well as the size of that core, depend on the DO level in the bulk liquid. A particular fixed granule size above which oxygen limitation occurs, cannot meaningfully be specified.

Fig. 3 shows the CLSM images of the stained phenol-granule probed at 360 μm from the outer surface. Most cells (total and dead), α- and β-polysaccharides, were accumulated in the outer layer of granules, whereas the protein and some cells formed a loosely structured core (Fig. 3). Fig. 4 combines the individual images obtained using the proposed stains. The distances indicated in Fig. 4 correspond to the depths from
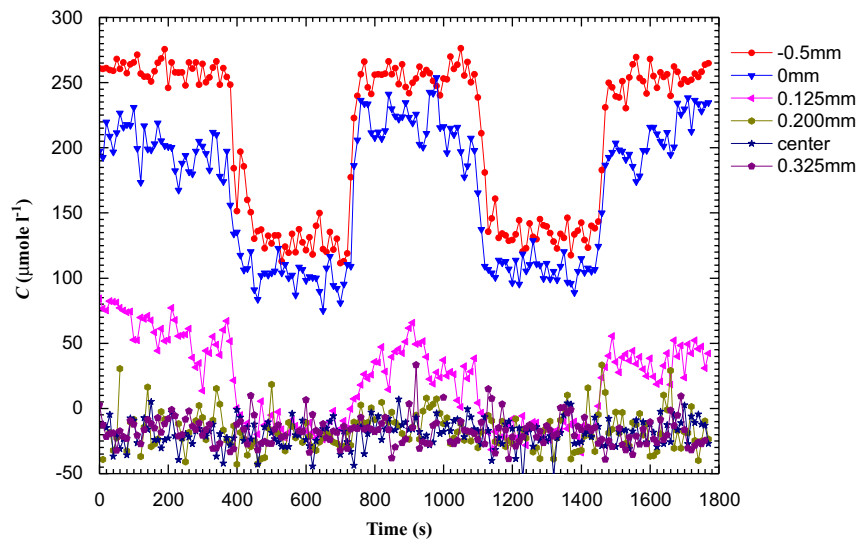
Fig. 2 – Microelectrode tests at different depths in the granule. Stepwise change in dissolved oxygen levels in surrounding water streams. Phenol-fed granule. 1.7 mm in diameter.
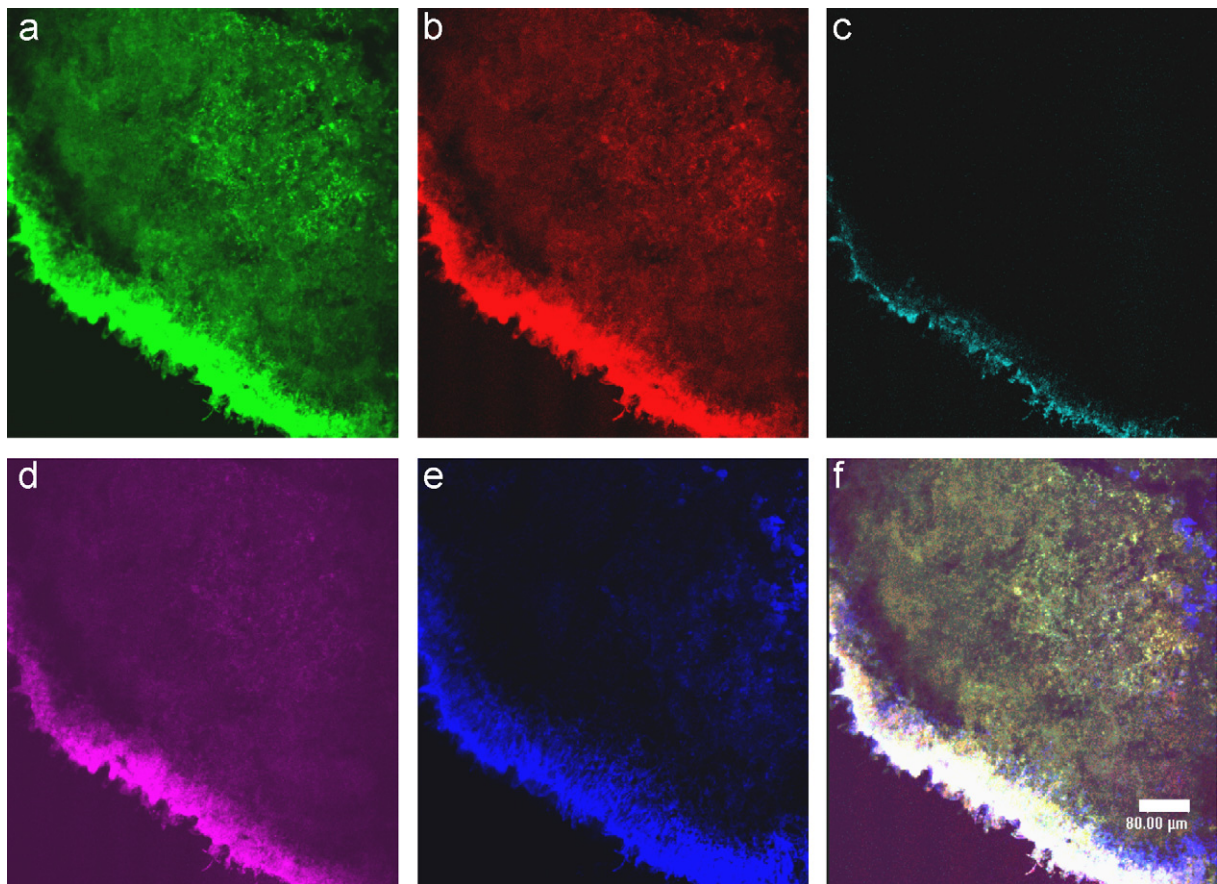

Fig. 3 – CLSM images for the phenol-fed granule. Bar = 80 μm. (a) CLSM image of protein (FITC), (b) CLSM image of total cells (SYTO 63), (c) CLSM image of α-D-glucopyranose polysaccharides (Con A), (d) CLSM image of dead cells (SYTOX Blue), (e) CLSM image of β-D-glucopyranose polysaccharides (calcofluor white), and (f) combined image of (a)–(e).

granule's surface the microelectrode tests in Fig. 2 were performed.

The phenol-fed granule has particular layers, as described by Tay et al. (2002a, b, c). Apparently, the granule is not of a uniform structure, as was assumed by Chiu et al. (2006). The outer layer of a phenol-fed granule is composed of cells, polysaccharides, and proteins; the inner core is a zone with a loose structure and low bioactivity. The CLSM observation
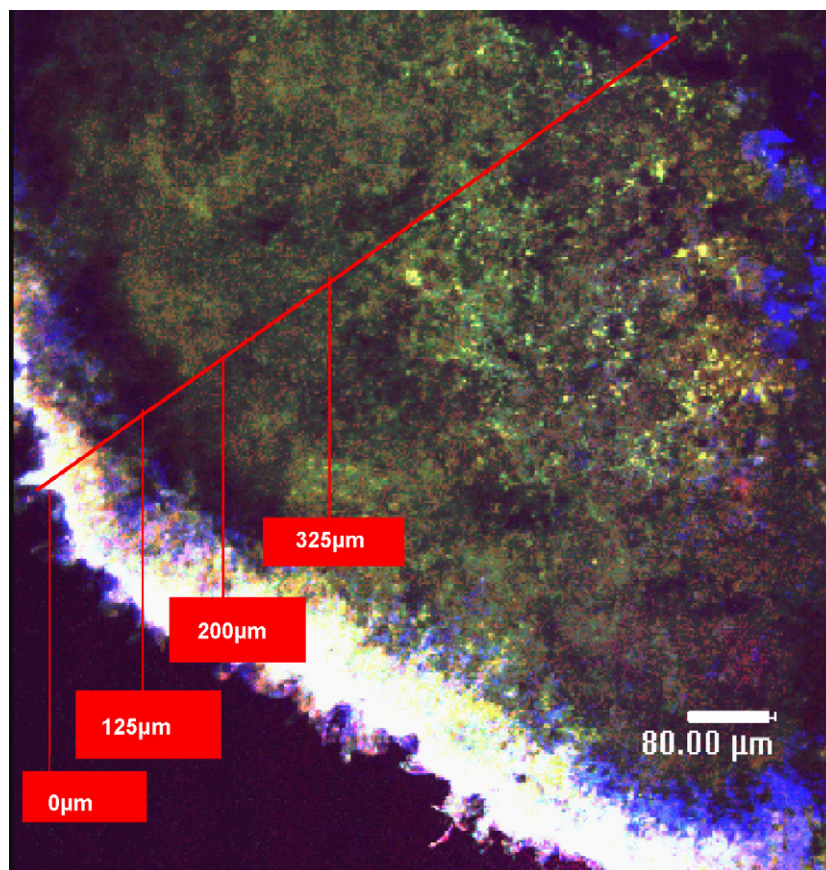
Fig. 4 – Combined CLSM images of phenol-fed granule. The distances indicated were the depths the microelectrode tests were performed.

corresponds to the noted DO decline in the surface layer of the granule in Fig. 2, in which many cells were accumulated. The DO drop in the second layer at depths of 125–375 μm is associated with some cells as noted in Fig. 3b, which are not present in large number, but may exhibit a high activity in the granules. These cells, however, face severe oxygen limitation at a bulk DO of approximately 150 μmol l^{-1} (4.8 mg l^{-1}), with which almost no oxygen is available after passing through the first active layer.

3.2.   DO levels and CLSM images in acetate-fed granule

Fig. 5 plots the DO concentrations measured at various positions outside and inside an acetate-fed granule using microelectrodes #1 and #2. The diameter of the granule was 3.10 mm and the upflow velocity was 2.4 mm s^{-1}, giving a Reynolds number of 7.4. The DO detected at 0.5 mm from the granule surface switched between those in bulk stream #A (300–310 μmol l^{-1}) and in bulk stream #B (90–100 μmol l^{-1}), and the DO values of the two streams are presented. The DO concentrations fell when moving toward the granule surface, because of the external mass transfer resistance of oxygen. The surface concentration of DO was of approximately 55% of in the bulk liquid. The DO fell monotonically with distance into the granule. When bulk water was saturated with oxygen

(stream #A), the DO was around 100 μmol l^{-1} at a depth of 125 μm, falling to close to zero at a depth of 250–500 μm. In stream #B with the reduced DO content, the DO level was around zero at a depth of 125 μm. An increase in bioactivity in the first surface layer (125 μm) was noted with time, and evidenced by the lower DO levels inside the granule after each switching. Over 1500–1800 s, most oxygen was consumed in the 125 μm layer, regardless of the bulk DO level. Therefore, whether oxygen limitation is serious depends on the local bioactivity, which can change with time and lead to different results in different stages, even in the same granule over a short testing time (30 min in this case).

Fig. 6 plots the results of fluorescent staining at 560 μm from the outer surface of the acetate-fed granule tested in Fig. 5. Cells and proteins were distributed more uniform over the acetate-fed granule's interior than the phenol-fed granule's interior (Fig. 3). The α-polysaccharides accumulated in the outer layer of the granules. Large pores were observed, but no specific layers were present, unlike in the phenol-fed granule. Restated, the interior of the acetate-fed granule resembled a uniform structure, as had been assumed by Chiu et al. (2006). Fig. 7 shows the depths where the DO measurements in Fig. 5 were conducted. The DO level declined over a thick surface layer with an initial thickness of 500 μm (Fig. 6). However, subsequently, the bioactivity of the first surface
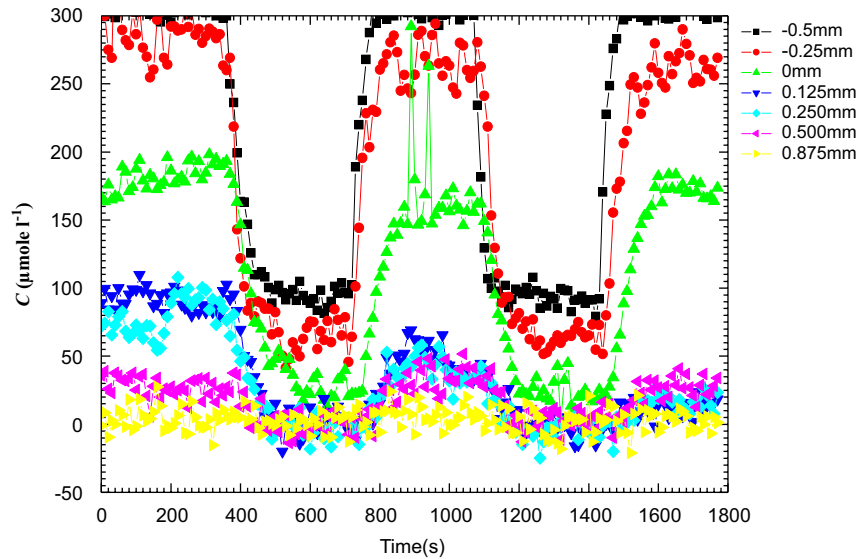
Fig. 5 – Microelectrode tests at different depths in the granule. Stepwise change in dissolved oxygen levels in surrounding water streams. Acetate-fed granule. 3.1 mm in diameter.
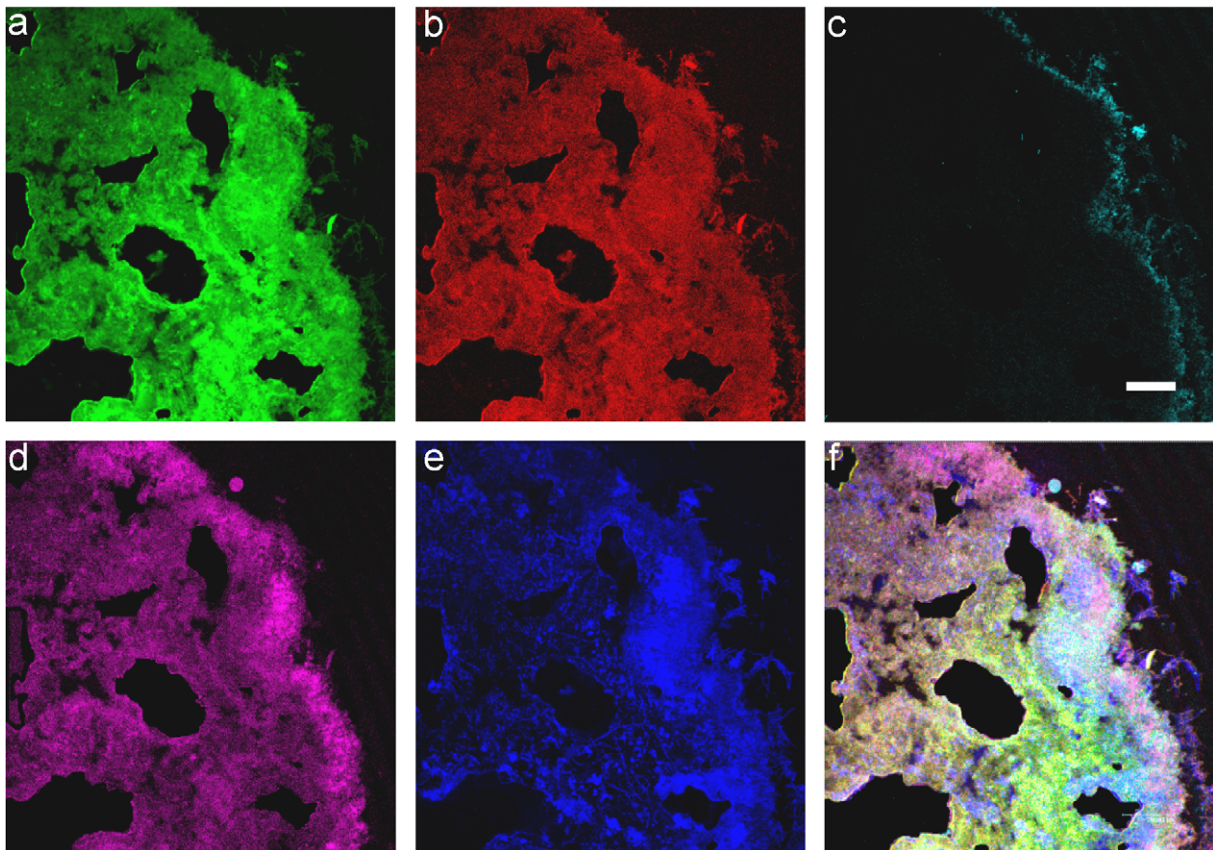

Fig. 6 – CLSM images for the acetate-fed granule. Bar = 200 μm. (a) CLSM image of protein (FITC), (b) CLSM image of total cells (SYTO 63), (c) CLSM image of α-D-glucopyranose polysaccharides (Con A), (d) CLSM image of dead cells (SYTOX Blue), (e) CLSM image of β-D-glucopyranose polysaccharides (calcofluor white), and (f) combined image of (a)–(e).

layer was considerably increased, yielding an almost anaerobic core at a depth of over 125 μm. The strictly aerobic microorganisms were greatly inhibited in the core regime. As in phenol-fed granule, most of the drop in DO occurred in the thin surface layer (Fig. 3) although cells were not confined therein.
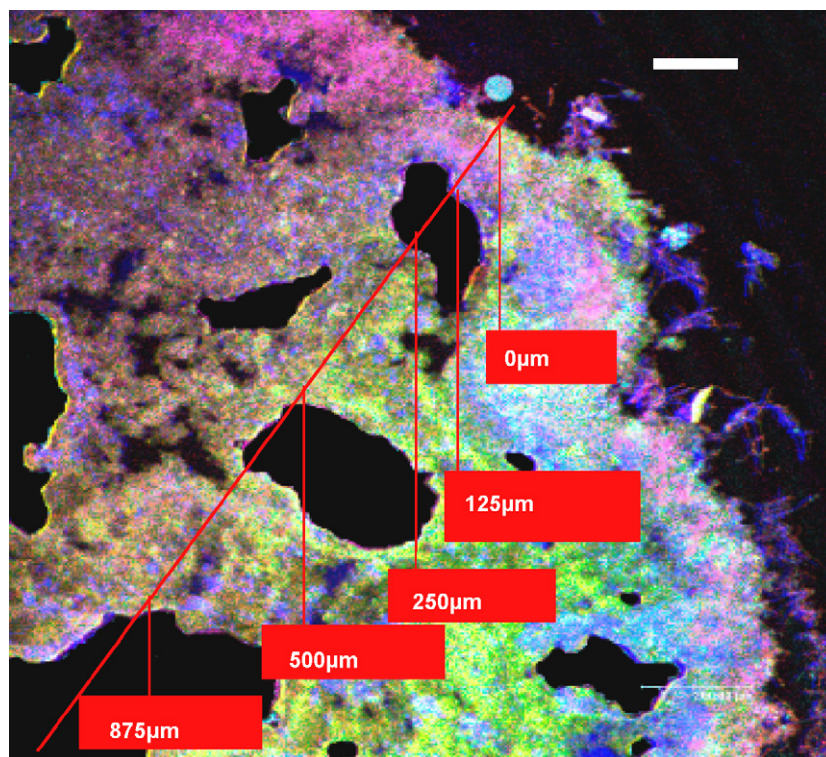
Fig. 7 – Combined CLSM images of acetate-fed granule. The distances indicated were the depths the microelectrode tests were performed.
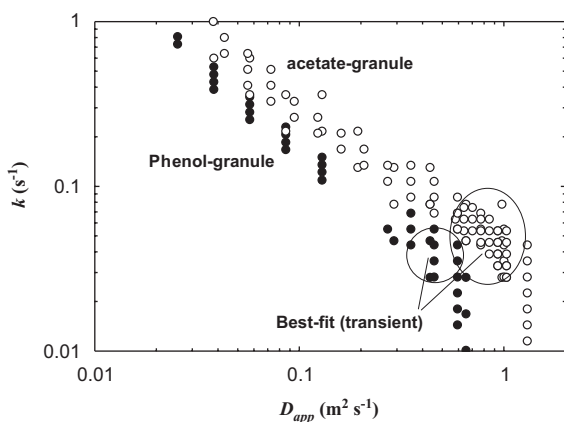

Fig. 8 – Best-fit k-D_{app} pairs for phenol-fed and acetate-fed granules based on steady-state and transient DO responses.

4.   Discussion

As shown in both Figs. 2 and 5, the surface layer with a thickness of 125 μm had a high bioactivity in both acetate-fed and phenol-fed granules, in which most diffusional oxygen frombulk liquid was consumed from the bulk liquid. This observation is consistent with the CLSM scans in Figs. 4 and 7, which reveal that most cells were present in the surface layer, such that the surface layer can consume oxygen. Therefore, in granules with high activity, as expected for active granules in adequately operated reactors, the oxygen limitation occurs at a radius of only 0.1 mm—much smaller than the 0.8 mm

suggested by Jang et al. (2003) or the 1 mm suggested by Li and Yu (2005).

Consider diffusion and reaction of oxygen in an active layer of thickness L, with the origin at the granule surface and the positive x-axis toward the granule center. The following transient, planar form approximates the governing equation for oxygen transport, since the layer thickness is only 17% of the radius of the phenol-fed granule, or 8% of that of the acetate-fed granule,

$$\frac{\partial C}{\partial t} = D_{app} \frac{\partial^2 C}{\partial x^2} - kC. \tag{1}$$

The boundary conditions are $C = C_s$ at $x = 0$ and $C = C_L$ at $x = L$, where C_s and C_L are the DO levels at the two ends and are recorded in experiments as functions of time; k is the rate constant.

In the steady state, the transient term in Eq. (1) is zero. The corresponding steady-state solution is as follows:

$$C = C_s \cos h(x\sqrt{k/D_{app}}) - C_s \frac{\sin h(x\sqrt{k/D_{app}})}{\tan h(L\sqrt{k/D_{app}})}$$
$$+ C_L \frac{\sin h(x\sqrt{k/D_{app}})}{\sin h(L\sqrt{k/D_{app}})}. \tag{2}$$

From this concentration distribution, the steady-state diffusional flux of oxygen at the granule surface ($x = 0$) is

$$N_A\big|_{x=0} = \sqrt{kD_{app}} \left(\frac{C_s}{\tan h(L\sqrt{k/D_{app}})} - \frac{C_L}{\sin h(L\sqrt{k/D_{app}})} \right). \tag{3}$$

At the granule surface, the oxygen flux by convection from the bulk should be equal to the diffusional flux into the

granule surface:

$$c(C_b - C_s) = N_A|_{x=0}, \quad (4)$$

where k_c is the mass transfer coefficient from the bulk liquid to the granule surface, and C_b is the bulk concentration of oxygen. The mass transfer coefficient in Eq. (4) is

$$Sh = \frac{k_c d}{D_{app}} = 2.0 + 0.6\, Re^{0.5}\, Sc^{1/3}, \quad (5)$$

where Sh and Sc are the Sherwood number and Schmidt number, respectively. $Sc = 435$ for water at $20\,°C$. At $Re = 4.4$ for a 1.7 mm phenol-fed granule, the corresponding k_c is $1.73 \times 10^{-5}\,\mathrm{m\,s^{-1}}$. The 3.1 mm acetate-fed granule at $Re = 7.48$ has $k_c = 1.54 \times 10^{-5}\,\mathrm{m\,s^{-1}}$.

Consider the mass balance of oxygen in the active layer:

$$4\pi R^2 N_A|_{x=0} - 4\pi (R - L)^2 N_A|_{x=L},$$
$$= \tfrac{4}{3}\pi \left(R^3 - (R-L)^3\right) k C_r, \quad (6)$$

where the mean oxygen concentration in layer L is,

$$C_r = \frac{\int_0^L C\,dx}{L}$$
$$= \frac{1}{L\sqrt{k/D_{app}}} \left\{ C_s \sin h\left(L\sqrt{k/D_{app}}\right) - \left[\left(\frac{C_s}{\tanh(L\sqrt{k/D_{app}})}\right.\right.\right.$$
$$\left.\left.\left. - \frac{C_L}{\sinh(L\sqrt{k/D_{app}})}\right)\left(\cos h\left(L\sqrt{k/D_{app}}\right) - 1\right)\right]\right\}. \quad (7)$$

Solving Eqs. (4), (6), (3) and (7), yields solutions for the pair k and D_{app} based on the steady-state DO data for a granule.

Fig. 8 plots the solutions for D_{app} and k based on steady-state DO data for the phenol-fed and acetate-fed granules, respectively. Infinitely many (D_{app}, k) pairs satisfy both Eqs. (5) and (7). Restated, these two values cannot be evaluated independently by fitting only steady-state solutions, as was noted by Beuling et al. (2000). Therefore, analysis, including the transient terms is required to verify these parameters.

Eq. (1) is difficult to solve analytically because both C_s at $x = 0$ and C_L at $x = L$ are experimental data with random errors. A numerical solution was applied for parametric fitting. The central finite difference scheme was utilized to discretize Eq. (1). Initially ($t = t_1$), the following steady-state concentration profile was bounded by C_{s1} at $x = 0$ and C_{L1} at $x = L$, at the two ends:

$$C = C_{s1} \cos h\left(x\sqrt{k/D_{app}}\right) - C_{s1}\frac{\sin h(x\sqrt{k/D_{app}})}{\tan h(L\sqrt{k/D_{app}})}$$
$$+ C_{L1}\frac{\sin h(x\sqrt{k/D_{app}})}{\sin h(L\sqrt{k/D_{app}})}. \quad (8)$$

Then, after a period ($t = t_2$), or at 100–300 s in Figs. 2 and 5 based on experimental readings, another steady-state concentration distribution bounded by C_{s2} at $x = 0$ and C_{L2} at $x = L$, also at the ends, is obtained as follows:

$$C = C_{s2} \cos h\left(x\sqrt{k/D_{app}}\right) - C_{s2}\frac{\sin h(x\sqrt{k/D_{app}})}{\tan h(L\sqrt{k/D_{app}})}$$
$$+ C_{L2}\frac{\sin h(x\sqrt{k/D_{app}})}{\sin h(L\sqrt{k/D_{app}})} \quad (9)$$

Various (D_{app}, k) pairs in Fig. 8 were substituted into the numerical scheme to solve the transient equation (Eq. (1)) with the initial condition given by Eq. (8) and boundary conditions determined experimentally at $x = 0$ and L. With

appropriate parameters (D_{app}, k) set, the concentration distribution is consistent with Eq. (9) after the transient time used in the experiment.

A range of (D_{app}, k) pairs in Fig. 8 generates a steady-state concentration distribution given by Eq. (9), which is circled in Fig. 8. Restated, $D_{app} = (9.5 \pm 3.5) \times 10^{-10}\,\mathrm{m^2\,s^{-1}}$ and $k = (0.04 \pm 0.03)\,\mathrm{s^{-1}}$ for the acetate-fed granule, and $(3.5 \pm 1.0) \times 10^{-10}\,\mathrm{m^2\,s^{-1}}$ and $k = (0.055 \pm 0.025)\,\mathrm{s^{-1}}$ for the phenol-fed granule over the active layers. Accordingly, Li and Lu (2005) overestimated the oxygen diffusivity in their acetate-fed granule model.

The phenol-fed granule has a lower diffusivity of oxygen than does the acetate-fed granule, probably because of the higher mass transfer resistance of the former, reducing phenol toxicity. Based on an active layer with a thickness of 125 μm, the corresponding Thiele moduli are 1.0–2.2 for the phenol-fed granule, and 0.3–1.3 for the acetate-fed granule, revealing that the former has greater diffusional resistance than the latter. If the structural characteristics of the granule elucidated by CLSM scanning are neglected, then the oxygen diffusivity obtained by assuming a uniform porous granule would be much higher than that reported above, leading to errors of design and operation.

5. Conclusions

This work investigated the distributions of EPS and cells in the interiors of two aerobic granules, phenol-fed and acetate-fed, using a novel five-fold staining scheme combined with CLSM. The steady-state and transient DO levels at various depths in the granules with step changes in surrounding DO levels were recorded using microelectrodes. The interior of the phenol-fed granule was found to have a layered structure, in whose surface layer accumulated cells, proteins and polysaccharides with thickness of around 125 μm. Most oxygen transferred from bulk liquid was consumed over this surface layer of the phenol-fed granule. The EPS and cells were distributed throughout the entire interior of the acetate-fed granule. Most of the oxygen was also consumed by the first layer with a thickness of 125–375 μm; the thickness fell with cultivation time and a decline in the bulk DO level. Whether oxygen limitation in an aerobic granule system is of concern depends on the transport and reaction resistances of oxygen of a granule and the DO level of bulk liquid. According to this work, oxygen limitation was exhibited by granules with sizes of over 0.25 mm—smaller than reported in the literature.

A simplified one-dimensional model with two parameters, apparent diffusivity (D_{app}) and the rate constant (k) of the first-order reaction, was applied to describe the diffusion and reaction of oxygen in granules. These two model parameters could not be evaluated independently based on steady-state DO readings at various depths in granules. The best-fit (D_{app}, k) pairs that described both steady-state and transient DO responses of granules with step change in surrounding DO levels were evaluated using a numerical solution to the transient version of the model. The best-fit D_{app} of the active layer of acetate-fed granule was $(9.5 \pm 3.5) \times 10^{-10}\,\mathrm{m^2\,s^{-1}}$, and that for phenol-fed granule was $(3.5 \pm 1.0) \times 10^{-10}\,\mathrm{m^2\,s^{-1}}$. The diffusivity of oxygen in the phenol-fed granule was lower

than that for the acetate-fed granule probably because the denser layer structure of the former yielded a higher mass transfer resistance to toxic phenols.

REFERENCES

Beuling, E.E., Van Den Heuvel, J.C., Ottengraf, S.P.P., 2000. Diffusion coefficients of metabolites in active biofilms. Biotechnol. Bioeng. 67, 53–60.

Beun, JJ., Van Loosdrecht, MCM., Heijnen, JJ., 2002. Aerobic granulation in a sequencing batch airlift reactor. Water Res. 36, 702–712.

Chiu, Z.C., Chen, M.Y., Lee, D.J., Tay, S.T.L., Tay, J.H., Show, K.Y., 2006. Diffusivity of oxygen in aerobic granules. Biotechnol. Bioeng. 94, 505–513.

Chu, C.P., Lee, D.J., Tay, J.H., 2005. Floc model and intrafloc flow. Chem. Eng. Sci. 60, 565–575.

Cronenberg, C.C.H., Van Den Heuvel, J.C., 1991. Determination of glucose diffusion coefficient in biofilms with microelectrodes. Biosens. Bioelectron. 6, 255–262.

Di Iaconi, C., Ramadori, R., Lopez, A., Passino, R., 2005. Hydraulic shear stress calculation in a sequencing batch biofilm reactor with granular biomass. Environ. Sci. Technol. 39, 889–894.

Ivanov, V., Tay, J.H., Tay, S.T.L., Jiang, H.L., 2004. Removal of microparticles by microbial granules used for aerobic wastewater treatment. Water Sci. Technol. 50 (12), 147–154.

Jang, A., Yoon, Y.H., Kim, I.S., Kim, K.S., Bishop, P.L., 2003. Characterization and evaluation of aerobic granules in sequencing batch reactor. J. Biotechnol. 105, 71–82.

Jiang, H.L., Tay, J.H., Tay, S.T.L., 2002. Aggregation of immobilized activated sludge cells into aerobically grown microbial granules for the aerobic biodegradation of phenol. Lett. Appl. Microbiol. 35, 439–445.

Li, B., Bishop, P.L., 2004. Microprofiles of activated sludge floc determined using microelectrodes. Water Res. 38, 1248–1258.

Li, Y., Liu, Y., 2005. Diffusion of substrate and oxygen in aerobic granule. Biochem. Eng. J. 27, 45–52.

Liu, Y.Q., Liu, Y., Tay, J.H., 2005. Relationship between size and mass transfer resistance in aerobic granules. Lett. Appl. Microbiol. 40, 312–315.

McSwain, B.S., Irvine, R.L., Hausner, M., Wilderer, P.A., 2005. Composition and distribution of extracellular polymeric substances in aerobic flocs and granular sludge. Appl. Environ. Microbiol. 71, 1051–1057.

Morgenroth, E., Sherden, T., Van Loosdrecht, M.C.M., Heijnen, J.J., Wilderer, P.A., 1997. Aerobic granule sludge in a sequencing batch reactor. Water Res. 31, 3191–3194.

Moy, B.Y.P., Tay, J.H., Toh, S.K., Liu, Y., Tay, S.T.L., 2002. High organic loading influences the physical characteristics of aerobic sludge granules. Lett. Appl. Microbiol. 34, 407–412.

Mulder, R., Vereijken, T.L.F.M., Frijters, C.M.T.J., Vellinga, S.H.J., 2001. Future perspectives in bioreactor development. Water Sci. Technol. 44, 27–32.

Tay, J.H., Liu, Q.S., Liu, Y., 2001. Microscopic observation of aerobic granulation in sequential aerobic sludge blanket reactor. J. Appl. Microbiol. 91, 168–175.

Tay, J.H., Liu, Q.S., Liu, Y., 2002a. Characteristics of aerobic granules grown on glucose and acetate in sequential aerobic sludge blanket reactors. Environ. Tech. 23, 931–936.

Tay, J.H., Yang, S.F., Liu, Y., 2002b. Hydraulic selection pressure-induced nitrifying granulation in sequencing batch reactor. Appl. Microbiol. Biotechnol. 9, 332–337.

Tay, J.H., Ivanov, V., Pan, S., Tay, S.T.L., 2002c. Specific layers in aerobically grown microbial granules. Lett. Appl. Microbiol. 34, 254–257.

Tay, J.H., Tay, S.T.L., Ivanov, V., Pan, S., Liu, Q.S., 2003. Biomass and porosity profile in microbial granules used for aerobic wastewater treatment. Lett. Appl. Microbiol. 36, 297–301.

Toh, S.K., Tay, J.H., Moy, B.Y.P., Ivanoc, V., Ay, S.T.L., 2002. Size effect on the physical characteristics of the aerobic granule in a SBR. Appl. Microbiol. Biotechnol. 60, 687–695.